# Implicit Euler Implementation of Twisting Controller and Super-Twisting Observer without Numerical Chattering: Precise Quasi-Static MEMS Mirrors Control

*Dong* Luo[1], *Xiaogang* Xiong[2] , *Shanhai* Jin[3], *Wei* Chen[4]

[1] Wuhan National Laboratory for Optoelectonics, Huazhong University of Science and Technology, Wuhan 430074, China
[2] Harbin Institute of Technology (Shenzhen), 518055 Shenzhen, China
[3] School of Engineering, Yanbian University, Yanji 133002, China
[4] Shenzhen Institutes of Advanced Technology, Chinese Academy of Sciences, 518055 Shenzhen, China

**Abstract.** The quasi-static operations of MEMS mirror are very sensitive to undesired oscillations due to its very low damping. It has been shown that closed-loop control can be superior to reduce those oscillations than open-loop control in the literature. For the closed-loop control, the conventional way of implementing sliding mode control (SMC) algorithm is forward Euler method, which results in numerical chattering in the control input and output. This paper proposes an implicit Euler implementation scheme of super twisting observer and twisting control for a commercial MEMS mirror actuated by an electrostatic staggered vertical comb (SVC) drive structure. The famous super-twisting algorithm is used as an observer and twisting SMC is used as a controller. Both are discretized by an implicit Euler integration method, and their implementation algorithms are provided. Simulations verify that, as compared to traditional sliding mode control implementation, the proposed scheme reduces the chattering both in trajectory tracking output and control input in presence of model uncertainties and external disturbances. The comparison demonstrates the potential applications of the proposed scheme in industrial applications in terms of feasibility and performance.

## 1 Introduction

MEMS (Micro-electro-mechanical systems) mirrors are micro mechanical systems that can perform high dynamic and precise beam positioning for many applications such as 1D/2D light detection and ranging (LIDAR), tunable laser spectrometer and micro laser projection displays. In comparison with traditional laser beam positioning devices such as galvanometer scanners and deflection mirror driven by voice coil motor, MEMS scanners have the advantages of small size, high repeatability, rapid scanning frequency, light-weight and low power consumption. The low mass and dimensional make MEMS mirrors suitable for compact designs.

In recent years, the close-loop control shows its advantages over open-loop control in some aspects, such as larger bandwidth and robustness of the external dynamic effects. Increasing bandwidth of MEMS mirrors means it can perform higher speed scanning and deflection of laser beam. Robustness to external distur-bance indicates the trajectory and magnitude will be less affected by factors such as temperature changes and model uncertainties. Those advantages are desired for many applications. For example, MEMS mirror based LIDAR and micro laser projection display can be used as automotive sensor and head-up display, respectively, both of which need to keep its performances in very dynamical environments. Constructing a close-loop control needs the feedback signal of mirror angular position, which can be achieved onboard fabricated sensors such as piezo-resistivity or capacitances, or external sensors such as quad photodiode-based backside position sensor or PSD-based position detection module. The quality of feedback signal for various sensor fabrications can be very different and a robust control algorithm should be resistant to the feedback signal variance. This paper focus on sliding mode control to suppress the model uncertainties of MEMS mirror and external disturbance.

Sliding mode control (SMC) has been recognized as one of potentially useful control schemes due to its finite-time convergence, tracking accuracy and robustness against uncertainty [1], [2], [3]. In practice, the main drawback of SMC is numerical chattering which could cause damages to the actuators of systems and deteriorate the control performance. Several solutions have been proposed to alleviate the numerical chattering, such as higher order sliding mode (HOSM) [3], [4], adaptive sliding mode designs [5], [6], and implicit Euler methods [7], [8].

The HOSM is known to enable reduction of chattering by integrating the signum function just like the super- twisting algorithm. It, however, requires the derivatives of the sliding variable. It comes at the price

of tolerating only a smaller class of disturbance than the first order SMC. Furthermore, by implementing with the conventional forward Euler integration method, it can still suffer from severe chattering effects. The adaptive sliding mode is to render gains adaptive in the conventional SMC. Since the magnitude of chattering is proportional to the gains, the chattering effect can be reduced if the gains automatically fit themselves to perturbations the SMC needs to counteract. The adaptive SMC can reduce the numerical chattering but it cannot totally remove it.

This paper applies implicit Euler integration method to the conventional sliding mode control for the MEMS mirror close-loop control. The super twisting algorithm is employed to obtain the velocity estimation while the twisting SMC is used for the close-loop control of the MEMS mirror. Both are discretized by using implicit Euler integration method. It is the first time to apply the implicit Euler implementation of SMC to MEMS mirror control for reducing chattering and improving tracking performance. The present work is the first time to show implicit Euler integration for the twisting SMC based on graph of the multi-valued signum function sgn(•). Some researchers give the implementation of implicit Euler integration based on ZOH (Zero-Order Hold) discretization and AVI (Affine Variational Inequality) [9].

## 2 Problem statement

The aim is to track a desired deflection trajectory by controlling the applied driving voltage $v_1$ and $v_2$ at the comb electrodes. The relationship between the deflection angle and the voltages $v_1$ and $v_2$ is shown as Fig. 1. The physical model of the MEMS (Micro-electro-mechanical systems) mirrors is as follows [10]:

$$\dot{x}_1 = x_2 \tag{1a}$$

$$\dot{x}_2 = -\frac{b}{J}x_2 - \frac{\tau_s(x_1)}{J} + \underbrace{\frac{\tau_1+\tau_2}{J}}_{:=u^*} + \emptyset(t) \tag{1b}$$

where $x := (x_1, x_2) = (\theta, \dot{\theta})$ with the output $y := x_1 = \theta$, $\emptyset(t)$ represents external disturbances and model uncertain-ties, $J$ is the mirror inertia, $b$ linear viscous damping, and $\tau_s(x_1)$ is the nonlinear spring torque:

$$\tau_s(x_1) = \int_0^{x_1} \kappa(\bar{x}_1)\, d\bar{x}_1\,, \quad \kappa(x_1) = \kappa_0 + \kappa_2 x_1^2 \tag{2}$$

with positive linear spring coefficient $\kappa_0$, $\kappa_2 > 0$. Due to the dual comb structure of the MEMS mirror shown in Fig. 1(a), the input $u$ is split into two parts $\tau_i$, $i = 1,2$:

$$\tau_1 := \frac{1}{2}C_1'(\theta)v_1^2\,, \quad \tau_2 := \frac{1}{2}C_2'(\theta)v_2^2 \tag{3}$$

Where $C_i'(\theta), i = 1,2$ are the capacitance derivatives and can be approximated by using $\tau_s(\theta)$ and $V_i(\theta)$, i.e., $C_i'(\theta) = dC_i(\theta)/d\theta \approx \tau_s(\theta)/\bar{V}_i^2(\theta)$.

The open-loop control is achieved by using jerk-limited trajectory input. The raster scan of quasi-static axis of 2D scanner usually requires triangle trajectories or sawtooth trajectories. The jerk limited trajectories $\theta_d$ are designed as polynomials smooth functions with respect to the time $t$. The open-loop control is realized by rewriting (1) as

$$u_d = \ddot{\theta}_d + \frac{b}{J}\dot{\theta}_d + \frac{\tau_s(\theta_d)}{J} \tag{4}$$

The objective is to design a close-loop control with flatness-based feedforward to calculate the command voltages $(v_1, v_2)$ so that the $x_1$ can follow the desired trajectory $\theta_d$ with small mean tracking error and high repeatability. The designed control $u^*$ is the sum of feedforward $u_d$ and feedback control $u$:

$$u^* = u_d + u \tag{5}$$

It should be noted that due to the staggered comb design, only an unidirectional torque can be produced. This means, the mirror combs can only pull but not push the mirror. This leads to a switch structure for the control design. A comb switch toggles between the comb electrode according to the sign of the desired generalized input $u^*$ as follows:

$$v_1(u^*, \hat{\theta}_d) = \begin{cases} \sqrt{\dfrac{2Ju^*}{C_1'(\hat{\theta}_d)}}, & if\ u^* > 0 \\ 0, & if\ u^* \le 0 \end{cases} \tag{6}$$

$$v_2(u^*, \hat{\theta}_d) = \begin{cases} 0, & if\ u^* > 0 \\ \sqrt{\dfrac{2Ju^*}{C_2'(\hat{\theta}_d)}}, & if\ u^* \le 0 \end{cases} \tag{7}$$

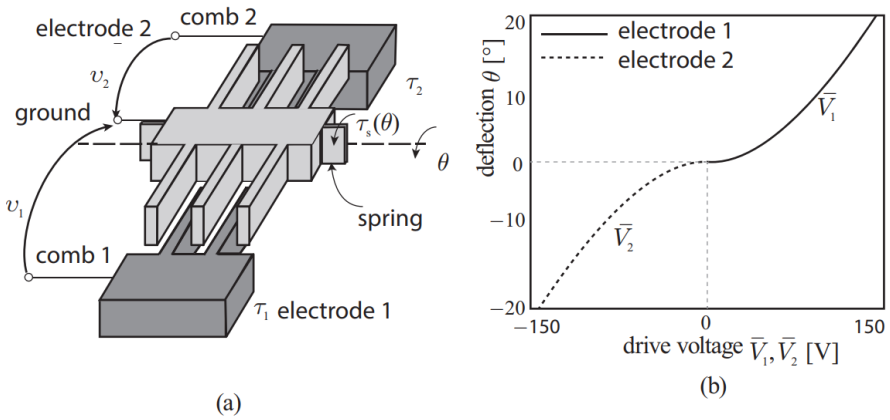


**Fig. 1.** Quasistatic-resonant micro-scanner chip [10]; (a) Principal design of quasi-static staggered vertical comb drive (b) Static voltage deflection characteristic.

## 3 Close-loop control design with implicit Euler implementation

### 3.1 Observer design and its implementation

The observer for (1) is designed as the super-twisting algorithm (STA):

$$\dot{\hat{x}}_1 = \hat{x}_2 + \alpha\lfloor z_1\rceil^{\frac{1}{2}} \quad (8a)$$

$$\dot{\hat{x}}_2 = -\frac{b}{J}\hat{x}_2 - \frac{\tau_S(x_1)}{J} + u^* + \beta\lfloor z_1\rceil^0 \quad (8b)$$

where $\hat{x} := [\hat{x}_1\,,\ \hat{x}_2]^T$ is the estimation of $x := [x_1\,,\ x_2]^T$, $\alpha,\ \beta$ are positive constants, $\lfloor\bullet\rceil^r := |\bullet|^r sgn(\bullet)\,, r \in \mathbb{R}_+$. $z_i := x_i - \hat{x}_i\,, i = 1,2$, represent the estimation errors. The error dynamics is as follows:

$$\dot{z}_1 = z_2 - \alpha\lfloor z_1\rceil^{\frac{1}{2}} \quad (9a)$$

$$\dot{z}_2 = -\beta\lfloor z_1\rceil^0 + \rho \quad (9b)$$

where ρ represents the residual errors. It has been shown that for appropriate parameters $\alpha,\ \beta > 0$, $z_i := x_i - \hat{x}_i\,, i = 1,2$, converge to the origin in finite time, which means $\hat{x}_i = x_i\,,\ i = 1,2$. The conventional explicit Euler implementation is as follows:

$$z_{1,k+1} = z_{1,k} + h(z_{2,k} - \alpha\lfloor z_{1,k}\rceil^{\frac{1}{2}}) \quad (10a)$$

$$z_{2,k+1} = z_{2,k} + h(-\beta\lfloor z_{1,k}\rceil^0 + \rho_k) \quad (10b)$$

where $\mathrm{h} = t_{k+1} - t_k > 0$ represents the fixed sampling period, the notation $z_{i,k}$ stands for $z_i(t_k)$. However, due to the numerical chattering caused by $\beta\lfloor z_{1,k}\rceil^0$, the accuracy of estimation can be affected. The key point of implementation of (8) is to calculate $z$, which is updated by (9). To suppress the numerical chattering effect on the estimation, here, the signum function $sgn(\cdot)$ is extended to a set-valued inclusion instead of single-valued function [9]:

$$\mathrm{sgn}(z_1) := \begin{cases} z_1/|z_1|\,, & \text{if } z_1 \neq 0 \\ [-1,1], & \text{if } z_1 = 0 \end{cases} \quad (11)$$

After applying an implicit Euler discretization to (9), the discrete-time version of the perturbed STA,

$$\bar{z}_{1,k+1} = z_{1,k} + h(\bar{z}_{2,k+1} - \alpha|z_{1,k}|^{\frac{1}{2}}\lfloor\bar{z}_{1,k+1}\rceil^0) \quad (12a)$$

$$\bar{z}_{2,k+1} \in \bar{z}_{2,k} + h(-\beta\lfloor\bar{z}_{1,k+1}\rceil^0) \quad (12b)$$

And $\bar{z}_{1,k+1}, \bar{z}_{2,k+1}$ are the normal states. From (12) one can derive the following inclusion:

$$\bar{z}_{1,k+1} \in z_{1,k} + h\bar{z}_{2,k} - (h\alpha|z_{1,k}|^{\frac{1}{2}} + h^2\beta)\lfloor\bar{z}_{1,k+1}\rceil^0 \quad (13)$$

Due to the inclusion symbol, (13) cannot be used in practical implantation. The following is the procedure to transfer (14) into an executable equation. Let $x, y \in \mathbb{R}^n$, $K \subset \mathbb{R}^n$ be a closed non empty convex set, and $M = M^T > 0$ be an $n \times n$ matrix. Then, one has the following relationship:

$$-x + y \in M^{-1}N_K(x) \Leftrightarrow x = \mathrm{proj}_M(K; y)$$

$$\Leftrightarrow x = \mathrm{argmin}_{z\in K}\frac{1}{2}(z-y)^T M(z-y) \quad (14)$$

Let $, y \in \mathbb{R}$, $K = [-1,1]$, one has

$$x \in sgn(y) \Leftrightarrow y \in N_{[-1,1]}(x) \quad (15)$$

By using the above relationships, finally, the algorithm for calculating $\hat{x}_1\,,\ \hat{x}_2$ is as following:

$$\varphi_k = z_{1,k} + h\bar{z}_{2,k}$$

$$\Gamma_k = h\alpha|z_{1,k}|^{\frac{1}{2}} + h^2\beta$$

$$\bar{z}_{1,k+1} = \varphi_k - \mathrm{proj}([-\Gamma_k, \Gamma_k]; \varphi_k)$$

$$\bar{z}_{2,k+1} = \bar{z}_{2,k} - \frac{h\beta}{\Gamma_k}\mathrm{proj}([-\Gamma_k, \Gamma_k]; \varphi_k)$$

$$\hat{x}_{1,k+1} = \hat{x}_{1,k} + h\hat{x}_{2,k} + \frac{h\alpha|z_{1,k}|^{\frac{1}{2}}}{\Gamma_k}\mathrm{proj}([-\Gamma_k, \Gamma_k]; \varphi_k)$$

$$\hat{x}_{2,k+1} = \hat{x}_{2,k} + h\left(-\frac{b}{J}\hat{x}_{2,k} - \frac{\tau_S(x_{1,k})}{J} + u_k^* + \frac{\beta}{\Gamma_k}\mathrm{proj}([-\Gamma_k, \Gamma_k]; \varphi_k)\right) \quad (16)$$

Where

$$\mathrm{proj}([-\Gamma_k, \Gamma_k]; \varphi_k) := \begin{cases} \Gamma_k & \text{if } \varphi_k > \Gamma_k \\ -\Gamma_k & \text{if } \varphi_k < -\Gamma_k \\ \varphi_k & \text{if } |\varphi_k| \leq \Gamma_k \end{cases} \quad (17)$$

*Remark 1*: To suppress the numerical chattering caused by $\beta\lfloor z_1\rceil^0$ in the observer (8) without scarifying the estimation accuracy, a normal error dynamical system (12) with state $\bar{z}_1$ and $\bar{z}_2$ is inserted here, instead of the actual system (10). It can be proved that after a finite step $k_0 > 0$, the normal state converges to the actual state, i.e., $|\bar{z}_{1,k} - z_{1,k}| \leq h^2\rho_k\,,\ \forall k > k_0 + 1$.

### 3.2 Twisting sliding mode control and its implementation

Let us recall the basics of the twisting algorithm for the case of a double integrator with a matched disturbance $\rho(t)$:

$$\dot{\sigma}_1 = \sigma_2 \quad (18a)$$

$$\dot{\sigma}_2 = u + \rho(t) \quad (18b)$$

where $\sigma_i \in \mathbb{R}\,, i = 1,2\ ,\ \mathrm{a} > \mathrm{b} > 0\ ,\ |\rho(t)| < W$ with some positive constant $W$, and u is the control input given as

$$u = -\mathrm{a}\lfloor\sigma_1\rceil^0 - \mathrm{b}\lfloor\sigma_2\rceil^0 \quad (19)$$

It has been proven that with appropriate gains $a,\ b$ with the knowledge of $W$, the state $\sigma_i\,, i = 1,2$ converge to the origin in finite time [9]. The traditional way of imple-mentation of (18) is

$$\sigma_{1,k+1} = \sigma_{1,k} + h\sigma_{2,k} \quad (20a)$$

$$\sigma_{2,k+1} = \sigma_{2,k} + h(\underbrace{-\mathrm{a}\lfloor\sigma_{1,k}\rceil^0 - \mathrm{b}\lfloor\sigma_{2,k}\rceil^0}_{u_k} + \rho_k) \quad (20b)$$

which results in numerical chattering in the input $u$ and output $\sigma_i$. The proposed procedure for implementation is as follows. Let us first consider the following implicit Euler discretization:

$$\bar{\sigma}_{1,k+1} = \sigma_{1,k} + h\bar{\sigma}_{2,k+1} \quad (21a)$$

$$\bar{\sigma}_{2,k+1} \in \sigma_{2,k} + h(-\mathrm{a}\lfloor\bar{\sigma}_{1,k+1}\rceil^0 - \mathrm{b}\lfloor\bar{\sigma}_{2,k+1}\rceil^0) \quad (21b)$$

For the case of $\sigma_{1,k} = 0$, (21) turns out to be the following formulation by using (14):

$$u_k = -\frac{1}{h}\mathrm{proj}([-h(a+b), h(a+b)]; \sigma_{2,k}) \quad (22a)$$

$$\bar{\sigma}_{2,k+1} = \sigma_{2,k} + hu_k \quad (22b)$$

$$\bar{\sigma}_{1,k+1} = h\bar{\sigma}_{2,k+1} \quad (22c)$$

Then, let us see the case $\sigma_{1,k} \neq 0$.With the relationship (14), one can obtain:

$$\mu_{1,k} \in -a\lfloor\bar{\sigma}_{1,k+1}\rceil^0, \mu_{2,k} \in -b\lfloor\bar{\sigma}_{2,k+1}\rceil^0 \quad (23a)$$

$$\mu_{2,k} = -\frac{1}{h}\text{proj}\big([-hb, hb]; \sigma_{2,k} + h\mu_{1,k}\big) \quad (23b)$$

$$\bar{\sigma}_{1,k+1} = \sigma_{1,k} + h\bar{\sigma}_{2,k+1} \quad (23c)$$

$$\bar{\sigma}_{2,k+1} = \sigma_{2,k} + h\mu_{1,k} - \text{proj}\big([-hb, hb]; \sigma_{2,k} + h\mu_{1,k}\big) \quad (23d)$$

By considering $\mu_{1,k}$ as a fixed value, as illustrated in Fig. 2, (23c) and (23d) can be transformed into $\bar{\sigma}_{1,k+1} = h(y_{1,k} - y_{2,k})$, with $y_{i,k}, i = 1,2$ definitions of functions of $\sigma_{2,k} + h\mu_{1,k}$ as follows:

$$y_{1,k} := \frac{\sigma_{1,k}}{h} + \sigma_{2,k} + h\mu_{1,k} \quad (24a)$$

$$y_{2,k} := \text{proj}\big([-hb, hb]; \sigma_{2,k} + h\mu_{1,k}\big) \quad (24b)$$

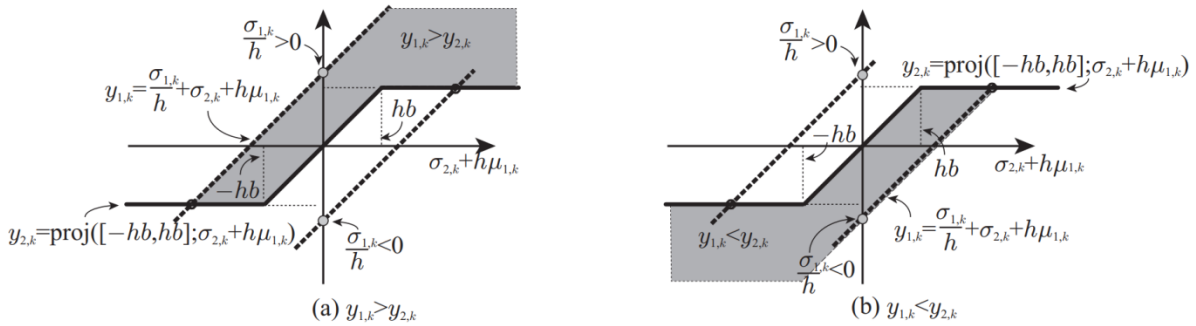


**Fig. 2.** Illustration of the implicit Euler integration method of (23)-(24).

## 4 Simulation validation

To validate the proposed algorithm with simulations, all parameters are set as the real experimental system of MEMS mirror described in [10]. A jerk-limited trajectory design is employed to reduce undesired oscillations:

$$\theta_{i+1}(t) = \bar{\theta}_i + \dot{\bar{\theta}}_i(t - t_i) + \ddot{\bar{\theta}}_i(t - t_i)^2 + \dddot{\bar{\theta}}_i(t - t_i)^3 \quad \text{for } t_i < t < t_{i+1} \text{ with } i = 0,1,\dots,n_{seg} - 1 \quad (26)$$

where $n_{seg}$ is the segmentation of the designed trajectory, $\bar{\theta}_i$, $\dot{\bar{\theta}}_i$, $\ddot{\bar{\theta}}_i$ and $\dddot{\bar{\theta}}_i$ are parameters defined the same in [10]. Let us design the sliding variable as $\sigma_1 := x_1 - \theta_d$. By defining $\dot{\sigma}_1 = \dot{x}_1 - \dot{\theta}_d := \sigma_2$, from (1), one can obtain the new dynamics as follows:

$$\dot{\sigma}_1 = \sigma_2 \quad (27a)$$

$$\dot{\sigma}_2 = \dot{x}_2 - \ddot{\theta}_d = -\frac{b}{J}x_2 - \frac{\tau_s(x_1)}{J} + \mu - \ddot{\theta}_d + \phi(t) \quad (27b)$$

Let us design the control as follows:

$$\mu = \frac{b}{J}\hat{x}_2 - \frac{\tau_s(\hat{x}_1)}{J} + \ddot{\theta}_d \underbrace{-a\lfloor\sigma_1\rceil^0 - b\lfloor\sigma_2\rceil^0}_{:=u} \quad (28)$$

where the first three terms are used as the equivalent control while $u$ is for sliding mode control. Substituting (28) into (27) leads to the formulation as (18) and the analysis follows that in Section 3.2. The control input $u$ is updated by using Algorithm 1.

From Fig.2, one can easily have $y_{1,k} = -hb$ if $\sigma_{1,k} > 0$ and $y_{1,k} = hb$ if $\sigma_{1,k} < 0$.

$$\mu_{1,k} = \begin{cases} \frac{1}{h^2}\big(-h^2 b - h\sigma_{2,k} - \sigma_{1,k}\big), & \text{if} \sigma_{1,k} > 0 \\ \frac{1}{h^2}\big(h^2 b - h\sigma_{2,k} - \sigma_{1,k}\big), & \text{if} \sigma_{1,k} < 0 \end{cases} \quad (25)$$

An algorithm can be extracted from the above analysis for calculating the control input $u_k$ and output $\bar{\sigma}_{i,k+1}$. The overall procedure above leads to Algorithm 1 that calculate $\mu_{i,k}$ and $\bar{\sigma}_{i,k+1}, i = 1,2$, by using an implicit Euler integration method illustrated in Fig. 2.

**Algorithm 1:** The procedure to calculate $\mu_{i,k}$ and $\bar{\sigma}_{i,k+1}, i = 1,2$ in (20)-(25), by using an implicit Euler intergration method illustrated in Fig. 2.

**input data**: $\sigma_{i,k}, i = 1,2$
**Parameter**: $h > 0, a > b > 0$
**begin**
  **if** $\sigma_{i,k} \neq 0$ **then**
    **if** $(\mu_{1,k} = -a) \wedge (y_{1,k} > y_{2,k})$ **then**
      $\mu_{1,k} = -a$ ;
    **else if** $(\mu_{1,k} = a) \wedge (y_{1,k} < y_{2,k})$ **then**
      $\mu_{1,k} = a$ ;
    **else**
      **if** $\sigma_{i,k} > 0$ **then**
        $\mu_{1,k} = \frac{1}{h^2}\big(-h^2 b - h\sigma_{2,k} - \sigma_{1,k}\big)$
      **end**
      **if** $\sigma_{i,k} < 0$ **then**
        $\mu_{1,k} = \frac{1}{h^2}\big(h^2 b - h\sigma_{2,k} - \sigma_{1,k}\big)$
      **end**
    $\mu_{2,k} = -\frac{1}{h}\text{proj}\big([-hb, hb]; \sigma_{2,k} + h\mu_{1,k}\big)$;
    $u_k = \mu_{1,k} + \mu_{2,k}$;
    $\bar{\sigma}_{1,k+1} = h\big(y_{1,k} - y_{2,k}\big)$;
    $\bar{\sigma}_{2,k+1} = \sigma_{2,k} + hu_k$;
  **end**
  **if** $\sigma_{1,k} == 0$ **then**
    $u_k = -\frac{1}{h}\text{proj}\big([-h(a+b), h(a+b)]; \sigma_{2,k}\big)$;
    $\bar{\sigma}_{2,k+1} = \sigma_{2,k} + hu_k$;
    $\bar{\sigma}_{1,k+1} = h\bar{\sigma}_{2,k+1}$;
  **end**
  $t_k \Leftarrow t_{k+1}$; $k \Leftarrow k + 1$;
**end**

The comparison is shown in Fig. 3. In Fig. 3(a)-(f), they results shown both explicit and implicit Euler integrations can track the desired trajectory. The acceleration rate is changed at crossing $\theta_{lin}$ points. Chattering means the actual angular is oscillated and unstable, which is a disaster to some precise instruments such as lidar and optical communicating system. Fig. 3(a)-(f) show that in the control input and control output, the chattering is drastically reduced by using the proposed implicit Euler method.

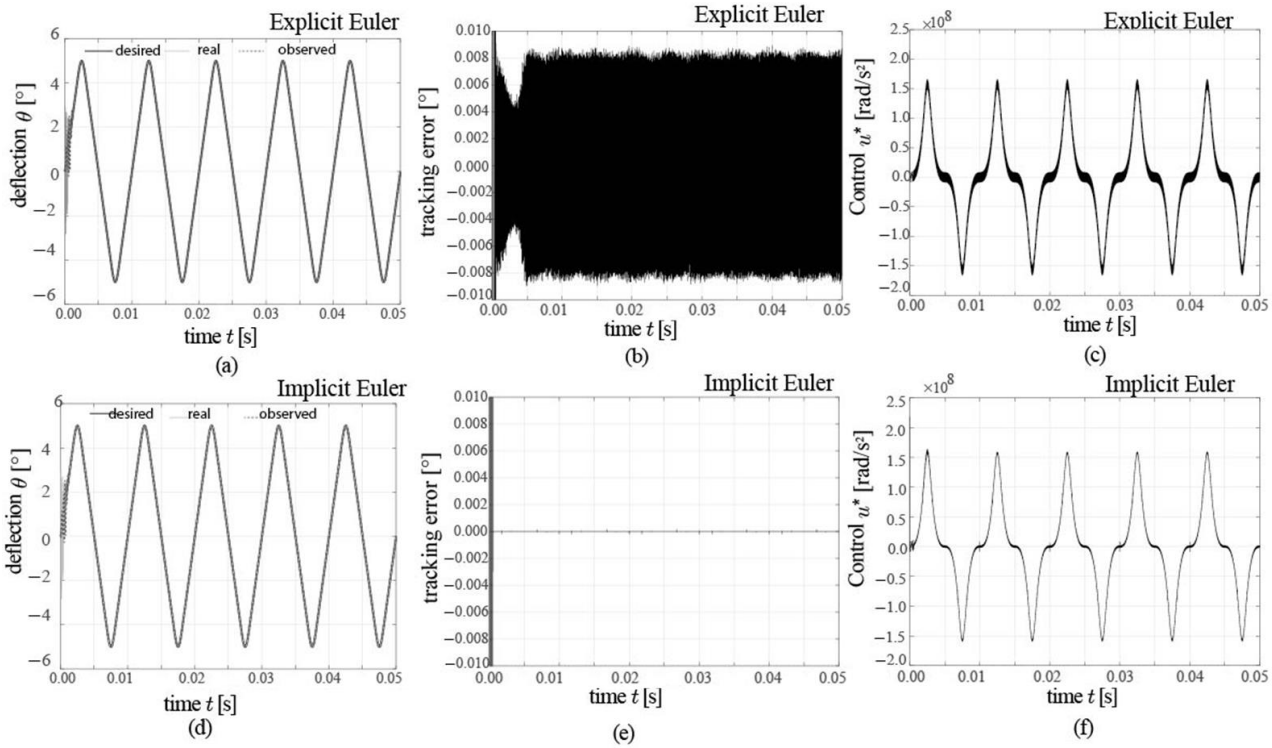


**Fig. 3.** Comparison of the proposed implicit Euler and conventional explicit Euler integrations of super twisting observer and twisting control.(a)(d) The desired trajectory tracking; (b)(e) The trajectory tracking error; (c)(f) The control input $u^* = u_d + u$. Other parameters are set as: J = $4.35\times10^{-12}$kgm$^2$, b = $5.21 * 10^{-11}$Nms, $\kappa_0 = 1.97 * 10^{-6}$Nm/rad, $\kappa_2 = 1.62 * 10^{-5}$Nm/rad$^3$, h = $10^{-6}$s, $\theta_{max} = 5°$, $\theta_{lin} = 4°$. The disturbance is set as $\phi(t) = \sin(40\pi t)$.The controller and observer gains are set as: $(a, b) = 5 \times 10^6(1, 2/3)$, $(\alpha, \beta) = \left(1.5 \times \sqrt{5 \times 10^3},\ 1.1 \times 5 \times 10^3\right)$.

## 5 Conclusion

This paper proposed an implicit Euler implementation algorithm for MEMS mirrors driven by the electrostatic staggered vertical comb (SVC) drive structure. The system model is a typical second order system and only the position or angular can be obtained. The velocity is observed by using the conventional super-twisting algorithm while its implementation is done by using the proposed implicit Euler method. The implicit Euler implementation for the twisting control is relative more complicate than that of super-twisting and therefore a special algorithm is introduced. The simulation results and comparison show that the proposed implicit Euler method is superior than the conventional explicit Euler method in term of chattering magnitude in both sliding mode control input and output.

Further study may focus on the proof of the convergence of the proposed implicit Euler integration and estimate the accuracy with disturbance existence. The experiments can be demonstrated with commercial MEMS mirrors integrated with some suitable angular position feedback sensor. Another interesting topic is to apply the proposed algorithm in other kind of higher order sliding mode control such as terminal sliding mode control with nested signum functions.

This work was finally supported by National Natural Science Foundation of China (No. 61605234) and Shenzhen Science and Technology Project (JCYJ20160531174039457). Project supported by a Grant for Key Research Items from the Ministry of Science and Technology of China (Grant No.2016 YFC1400701).

## References

1. J. Davila, L. Fridman, A. Levant, IEEE T. Automat. Contr. **50**, 11 (2005)
2. A. Levant, Int. J. Control. **58**, 6 (1993)
3. A. Levant, Automatica. **43**, 4 (2007)
4. A. Chalanga, S. Kamal, B. Bandyopadhyay, IEEE-ASME T. Mech. **20**, 5 (2015)
5. M. Taleb, F. Plestan, B. Bououlid, Int. J. Robust. Nonlin, **25**,8 (2015)
6. V. I. Utkin, A. S. Poznyak, Automatica. **49**, 1 (2013)
7. V. Acary, B. Brogliato, Y. V. Orlov, IEEE T. Automat. Contr. **57**, 5 (2012)

8. V. Acary, B. Brogliato, Syst. Control. Lett. **59**, 5 (2010)
9. O. Huber, V. Acary, B. Brogliato, F. Plestan, Control. Eng. Pract. **46** (2016)
10. R. Schroedter, M. Roth, K. Janschek, T. Sandner, Mechatronics. (2017)